Effect of inclusion of Hamiltonian dynamics to simulated annealing of reduced magnetohydrodynamics equilibrium calculations

M. Furukawa[1] and P. J. Morrison[2]

[1] Faculty of Engineering, Tottori University, Tottori 680–8552, Japan,
furukawa@tottori-u.ac.jp
[2] Department of Physics and Institute for Fusion Studies, University of Texas at Austin, Texas 78712, USA

Abstract. We have been developing a method, called simulated annealing (SA), to calculate equilibrium and stability of Hamiltonian systems. The artificial time evolution of SA is derived on the basis of Hamiltonian structure of the system, where the energy is changed monotonically while Casimir invariants are preserved. Since SA solves an initial-value problem for the equilibrium and stability calculations, it generally consumes time. We have examined whether the relaxation to the equilibrium can be accelerated by adding the original Hamiltonian dynamics to the SA dynamics for the low-beta reduced MHD system in cylindrical geometry. We have found that the inclusion of Hamiltonian dynamics can either accelerate or decelerate the relaxation compared to the pure SA case. In this paper, we show a case where the relaxation was decelerated. The decelerated time evolution of energy does not differ by the sign when adding the Hamiltonian dynamics. The deceleration occurred around when the kinetic energy became maximum. The sign of the flow part was found opposite depending on whether the Hamiltonian dynamics was added with a positive or a negative sign.

Keywords: simulated annealing, magnetohydrodynamics, Hamiltonian system

1 Introduction

Simulated annealing (SA)[1] is a kind of relaxation method for calculating equilibria of Hamiltonian systems. The SA is derived on the basis of the Hamiltonian structure, where the SA dynamics changes the energy of the system monotonically while Casimir invariants are preserved. We have applied SA for the low-beta reduced MHD[2] in a doubly-periodic rectangular geometry [3, 4] and in a cylindrical geometry[5], as well as for the high-beta reduced MHD[6] in a toroidal geometry[7]. For the MHD systems, especially considering magnetically-confined fusion plasmas, monotonic decrease of energy by SA leads to an energy minimum on a Casimir leaf, on which each Casimir invariant takes a same value.

The energy minimum on the Casimir leaf is an equilibrium of the system[8, 9]. Recently, SA was shown to be also usable for stability analyses [10].

The equilibrium and stability calculations by SA consume time generally, since we need to solve an initial-value problem. We have developed a method to accelerate relaxation to an equilibrium in [10]. Here, we examine another method; whether the relaxation can be accelerated by adding the original Hamiltonian dynamics is added to the SA dynamics.

The paper is organized as follows. In Sec. 2, the governing equations are presented. Section 3 shows numerical results of time evolution by mixed Hamiltonian and SA dynamics. Conclusions are given in Sec. 4.

2 Governing equations

Let us consider a cylindrical plasma with its minor radius a and the length $2\pi R_0$. We use cylindrical coordinates (r, θ, z). The dissipation-less, low-beta reduced magnetohydrodynamics (MHD)[2] is the Hamiltonian system that we adopt in this study:

$$\frac{\partial U}{\partial t} = [U, \varphi] + [\psi, J] - \varepsilon \frac{\partial J}{\partial \zeta}, \tag{1}$$

$$\frac{\partial \psi}{\partial t} = [\psi, \varphi] - \varepsilon \frac{\partial \varphi}{\partial \zeta}, \tag{2}$$

where Eq. (1) is the vorticity equation and Eq. (2) is the Ohm's law. These equations are normalized by using typical values of physical quantities. The fluid velocity is given by $\boldsymbol{u} := \hat{\boldsymbol{z}} \times \nabla \varphi$, where φ is the stream function and $\hat{\boldsymbol{z}}$ is the unit vector along the z axis. The vorticity U is defined by $U := \hat{\boldsymbol{z}} \cdot \nabla \times \boldsymbol{u} = \triangle_\perp \varphi$, where $\triangle_\perp$ is the two-dimensional Laplacian on the r–θ plane. Similarly, the magnetic field is given by $\boldsymbol{B} := B_0 \hat{\boldsymbol{z}} + \nabla \psi \times \hat{\boldsymbol{z}}$ with $B_0 = 1$ by normalization, and $J := -\hat{\boldsymbol{z}} \cdot \nabla \times \boldsymbol{B} = \triangle_\perp \psi$. The Poisson bracket is defined by $[f, g] := \hat{\boldsymbol{z}} \cdot \nabla f \times \nabla g$ for arbitrary functions f and g. The inverse aspect ratio is defined as $\varepsilon := a/R_0$. The toroidal angle coordinate $\zeta := z/R_0$ is also used.

The governing equations can be written in a Hamiltonian form. Since the Poisson bracket is skew-symmetric, the energy of the system is conserved. Also, the noncanonical Poisson bracket introduces Casimir invariants[11]. An example of the Casimir invariant is the magnetic helicity.

The SA equations adopted in this study are the following:

$$\frac{\partial U}{\partial t} = [U, \tilde{\varphi}] + [\psi, \tilde{J}] - \varepsilon \frac{\partial \tilde{J}}{\partial \zeta}, \tag{3}$$

$$\frac{\partial \psi}{\partial t} = [\psi, \tilde{\varphi}] - \varepsilon \frac{\partial \tilde{\varphi}}{\partial \zeta}, \tag{4}$$

where the advection fields are replaced from the original low-beta reduced MHD equations as

$$\tilde{\varphi}(\boldsymbol{x},t) := -\alpha_{11}\int_{\mathcal{D}} \mathrm{d}^3x'\, g(\boldsymbol{x},\boldsymbol{x}')f^1(\boldsymbol{x}',t), \tag{5}$$

$$\tilde{J}(\boldsymbol{x},t) := -\alpha_{22}\int_{\mathcal{D}} \mathrm{d}^3x'\, g(\boldsymbol{x},\boldsymbol{x}')f^2(\boldsymbol{x}',t). \tag{6}$$

Here f^1 is the right-hand side of Eq. (1), and f^2 is the right-hand side of Eq. (2). The kernel g is a three-dimensional Green's function satisfying $\triangle g(\boldsymbol{x},\boldsymbol{x}') := -\delta^3(\boldsymbol{x},\boldsymbol{x}')$, and α_{11} and α_{22} are chosen to be constants. The derivation of the SA equations (3) and (4) is based on the double bracket formulation of SA [1], although the choice of the advection fields Eqs. (5) and (6) can be more general. Note that the SA equations (3) and (4) have the same form as the original equations (1) and (2). Since the Casimir invariants are generated by the properties of the Poisson bracket, the SA dynamics preserves the Casimir invariants of the original dynamics.

Now, let us show the equations that we solve in this study:

$$\frac{\partial U}{\partial t} = \tilde{f}^1 + cf^1, \tag{7}$$

$$\frac{\partial \psi}{\partial t} = \tilde{f}^2 + cf^2, \tag{8}$$

where $\tilde{f}^1$ is the right-hand side of Eq. (3), and $\tilde{f}^2$ is the right-hand side of Eq. (4). The constant c represents how much the original Hamiltonian dynamics is added to the SA dynamics. We solved Eqs. (7) and (8) by using Fourier decomposition in θ and ζ directions. Positive c adds forward Hamiltonian dynamics, while negative c adds it backwards.

3 Numerical results

In this section, numerical results are shown, where the inclusion of the Hamiltonian dynamics caused deceleration of relaxation. Note that we also found a case where the relaxation was accelerated compared to the pure SA case. It is a future issue to clarify in what condition the relaxation is accelerated or decelerated. This will be reported elsewhere.

The cylindrically symmetric equilibrium we chose for this study has $\varepsilon = 1/10$ and has no flow. The safety factor profile is shown in Fig. 1. If we decompose a perturbed quantity in a Fourier series in θ and ζ, the corresponding mode numbers $(m,n) = (2,1)$ and those with the same m/n are in resonance at the $q = 2$ surface at $r = 1/2$.

This equilibrium was perturbed by the resonant components, while staying on the same Casimir leaf as the cylindrically symmetric equilibrium. This was realized by solving Eqs. (3) and (4) under fixed advection fields $\tilde{\varphi}$ and $\tilde{J}$ with the mode numbers $(m,n) = (2,1)$, but not related to the SA formulation as Eqs. (5) and (6).

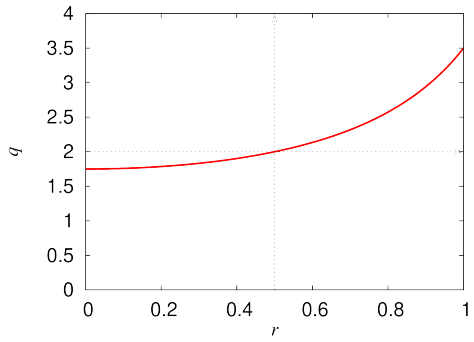

Fig. 1: Safety factor profile of the unperturbed equilibrium.

Figure 2 shows time evolutions of the total energy, summation of the kinetic energy $E_{\rm k}$ and the magnetic energy $E_{\rm m}$, for various ratios c of inclusion of Hamiltonian dynamics to the SA. The fastest relaxation was achieved for $c = 0$; the inclusion of the Hamiltonian dynamics decelerated the relaxation for this case. Larger $|c|$ yielded earlier start of deceleration.

Moreover, as observed in Fig. 2, we found no difference in the energy evolutions with positive and negative cs with a same absolute value. Although the energy evolutions are almost same, however, they are actually different. This will be discussed later in this paper. Note that the overlap of the energy evolution is accidental; we obtained a case where energy evolution do not overlap each other for positive and negative cs with a same absolute value. We need to further examine in what case the energy evolution almost overlap each other or deviate between positive and negative cs with a same absolute value. This will be reported elsewhere.

Let us examine when the relaxation started to slow down. For example, it became visible at around $t \simeq 10$ for $c = \pm 10$. Figure 3 shows the time evolution of the kinetic energy $E_{\rm k}$ for $c = \pm 10$. The kinetic energy $E_{\rm k}$ became maximum at $t \simeq 20$ for both signs of c, although $E_{\rm k}$ is still small. The slow down became visible a little bit earlier timing than the $E_{\rm k}$ maximum. We examined the cases with other cs, and found that the deceleration of relaxation started visible a little bit earlier than the timing of the kinetic energy maximum.

We observed the time evolutions of maximum typical values of Fourier components of $\tilde{f}^1$, cf^1, $\tilde{f}^2$, and cf^2 shown in Fig. 4. For example, $\max_{r,m,n} |\tilde{f}^1_{m,n}(r,t)|$ is the maximum absolute value of $\tilde{f}^1_{m,n}(r,t)$ among every r, m and n at each instance. The energy can be changed by the SA components $\tilde{f}^1$ and $\tilde{f}^2$, and they indeed became small at $t \simeq 20$, which is the timing of maximum $E_{\rm k}$. Note that the components of original Hamiltonian dynamics without tildes do not affect the energy evolution directly, although $\max_{r,m,n} |f^1_{m,n}(r,t)|$ is always significantly larger than the others.

Let us now show a difference between positive and negative cs. Figures 5a and 5c shows the helical component of vorticity U on the r–θ plane at $t \simeq 100$;

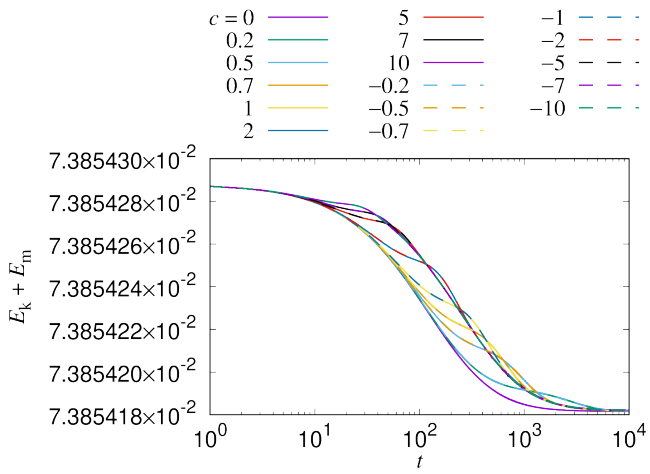

Fig. 2: Time evolution of total energy. The purple curve with the lowest energy throughout shows the case of $c = 0$; inclusion of original Hamiltonian dynamics to SA, where c is the ratio, decelerated relaxation to the equilibrium for this case. Time evolutions of energy with positive and negative cs with a same absolute value almost overlapped each other. Larger $|c|$ yielded earlier start of deceleration.

U was Fourier reconstructed without the $(m, n) = (0, 0)$ component. Also Figs. 5b and 5d shows the helical component of magnetic flux function ψ at the same timing. We observe that U has a opposite sign depending on the sign of c, while ψ has the same sign for both positive and negative cs.

This can be explained as follows. The difference depending on c can only occur by the terms cf^1 and cf^2 in Eqs. (7) and (8), respectively. Thus we focus on behaviors of f^1 and f^2. First, let us remind readers that the $\varepsilon\partial/\partial\zeta$ terms in f^1 and f^2 can be included in the Poisson bracket terms by introducing a helical flux $\psi_{\mathrm{h}} := \psi + \varepsilon r^2/(2q_{\mathrm{s}})$ in single helicity situations, where q_{s} is the safety factor at the resonant surface. Therefore, we observe the behaviors of the Poisson bracket terms. The terms $[U, \varphi]$ and $[\psi, J]$ are both squared terms of flow and magnetic components, respectively. Thus, the sign of these Poisson bracket terms, and also f^1, has the same sign even if the flow or magnetic component itself has an opposite sign due to the sign difference of c. Then, $\partial U/\partial t$ due to the cf^1 term has an opposite sign depending on the sign of c, leading to the opposite sign of U. On the other hand, the Poisson bracket term $[\psi, \varphi]$ is a product of flow and magnetic components. Since U has opposite signs for positive and negative cs, φ also has the opposite signs. Then f^2 has opposite signs for positive and negative cs if ψ has the same sign. If the last assumption is true, cf^2 has a same sign for positive and negative cs, and thus $\partial\psi/\partial t$ has the same sign for both cs. Then the sign of ψ is the same for both cs, which is consistent with the last assumption.

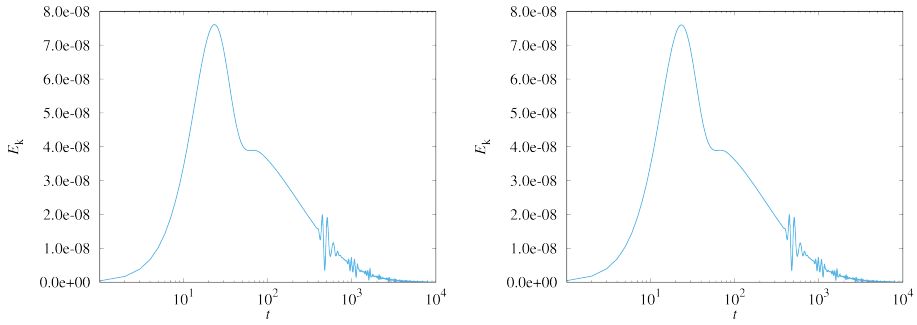

(a) $c = 10$. (b) $c = -10$.

Fig. 3: Time evolution of kinetic energy E_k. The deceleration of energy decrease started visible when E_k became maximum.

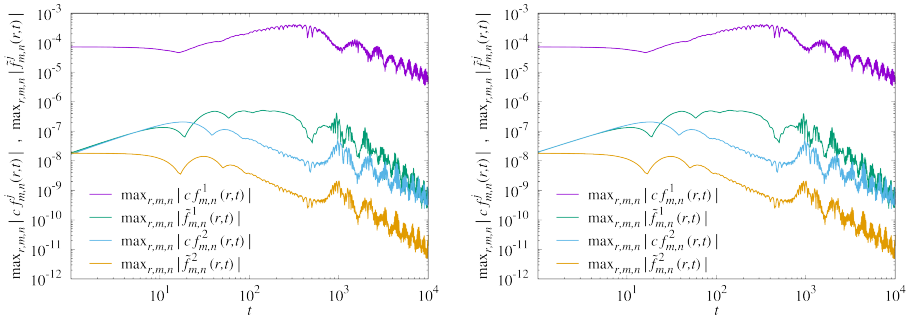

(a) $c = 10$. (b) $c = -10$.

Fig. 4: Time evolution of maximum typical values of Fourier components of $\tilde{f}^1$, cf^1, $\tilde{f}^2$, and cf^2.

This sign difference remained through the end of the simulation. For example, Fig. 6 shows the helical components of U and ψ at the final time of the simulation $t = 10^4$.

4 Conclusions

Forward or backward Hamiltonian dynamics was added to the simulated annealing (SA) dynamics to examine whether the relaxation to an equilibrium can be accelerated. In the presented case, the addition of Hamiltonian dynamics rather slowed down the relaxation. The deceleration started to be visible a little bit earlier than when the kinetic energy became maximum. The decelerated time evolutions almost overlapped between cases where forward or backward Hamiltonian dynamics added with a same magnitude. However, the flow components had an opposite sign depending on the sign of the added Hamiltonian dynamics,

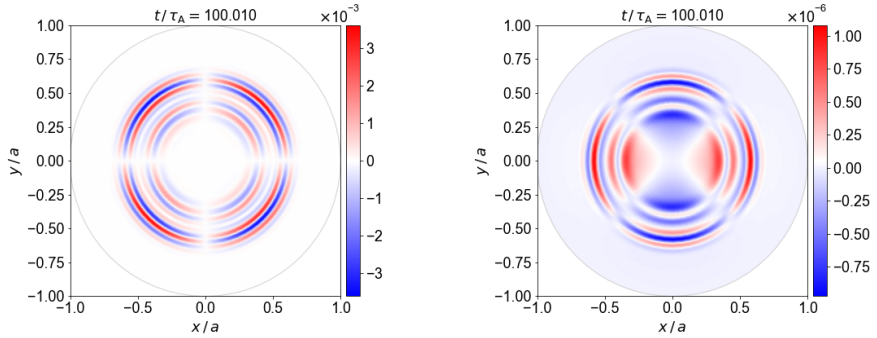

(a) $c = 10$, helical component of U.

(b) $c = 10$, helical component of ψ.

(c) $c = -10$, helical component of U.

(d) $c = -10$, helical component of ψ.

Fig. 5: Helical components of U and ψ on the r–θ plane at $t \simeq 100$. The sign of U is opposite for positive and negative cs, while the sign of ψ is the same.

while the magnetic components had a same sign. This sign difference was explained by examining the behavior of the Poisson bracket terms of the governing equations.

Acknowledgement

M.F. was supported by JSPS KAKENHI Grant Number JP21K03507, while P.J.M. was supported by USDOE DE-FG05–80ET-53088.

References

1. G. R. Flierl, P. J. Morrison, Physica D **240**, 212 (2011).
2. H. R. Strauss, Phys. Fluids **19**, 134 (1976).
3. Y. Chikasue and M. Furukawa, Phys. Plasmas **22**, 022511 (2015).
4. Y. Chikasue and M. Furukawa, J. Fluid Mech. **774**, 443 (2015).

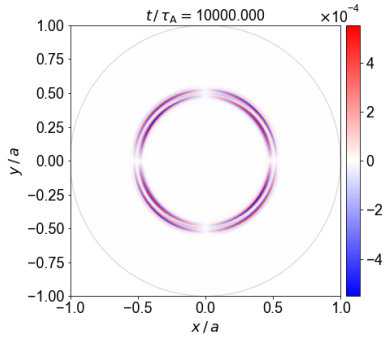

(a) $c = 10$, helical component of U.

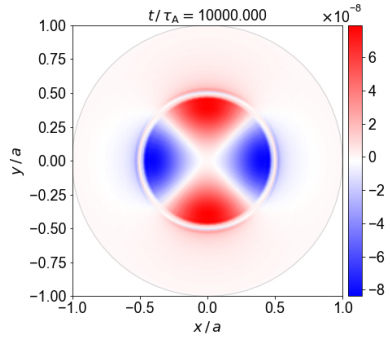

(b) $c = 10$, helical component of ψ.

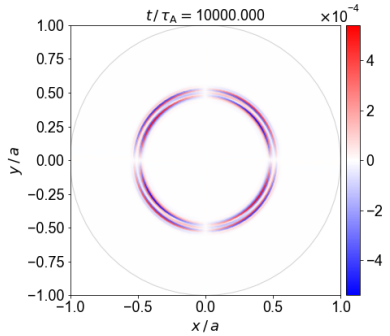

(c) $c = -10$, helical component of U.

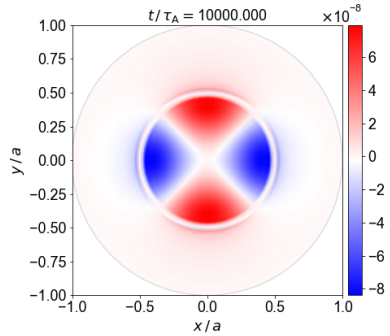

(d) $c = -10$, helical component of ψ.

Fig. 6: Helical components of U and ψ on the r–θ plane at $t = 10^4$. The sign of U is opposite for positive and negative cs, while the sign of ψ is the same.

5. M. Furukawa and P. J. Morrison, Plasma Phys. Control. Fusion **59**, 054001 (2017).
6. H. R. Strauss, Phys. Fluids **20**, 1354 (1977).
7. M. Furukawa, Takahiro Watanabe, P. J. Morrison, and K. Ichiguchi, Phys. Plasmas **25**, 082506 (2018).
8. M. D. Kruskal and C. R. Oberman, Phys. Fluids **1**, 275 (1958).
9. V. I. Arnol'd, Prikl. Math. Mech. **29**, 846 (1965), [English transl. *J. Appl. Maths Mech.* **29**, 1002–1008 (1965)].
10. M. Furukawa and P. J. Morrison, Phys. Plasmas **29**, 102504 (2022).
11. P. J. Morrison, Rev. Mod. Phys. **70**, 467 (1998).